Observations of wave-generated vortex ripples on the North Carolina continental shelf

Fabrice Ardhuin
Centre Militaire d'Océanographie, Service Hydrographique et Océanographique de la Marine, Brest, France

T. G. Drake
Department of Marine, Earth and Atmospheric Sciences, North Carolina State University, Raleigh, North Carolina, USA

T. H. C. Herbers
Oceanography Department, Naval Postgraduate School, Monterey, California, USA

Received 18 May 2001; revised 15 November 2001; accepted 4 December 2001; published XX Month 2002.

[1] Sand ripples with wavelengths between 0.5 and 3 m were observed on the bottom across the U.S. east coast continental shelf off North Carolina during three side-scan sonar surveys in September and December 1999. Ripples were present in about 75% of the survey images, in particular, in regions with coarser sediments. Analysis of surficial sediment samples shows that median grain diameters range from 0.1 to 4.7 mm with large variations on the inner shelf over distances ¡1 km. The observed ripple properties are consistent with wave-generated vortex ripples. Analysis of concurrent wave observations indicates that the ripple crests were aligned perpendicular to the average direction of near-bottom wave-induced motions during preceding events that were sufficiently energetic to mobilize surficial sediments. Furthermore, the ripple wavelengths proportionality to near-bottom wave orbital excursions is consistent with wave-formed vortex ripples. These findings support the hypothesis that the observed strong attenuation of waves across the shelf resulted from form drag over large vortex ripples. *INDEX TERMS:* 3022 Marine Geology and Geophysics: Marine sediments—processes and transport; 3045 Marine Geology and Geophysics: Seafloor morphology and bottom photography; 4211 Oceanography: General: Benthic boundary layers; 4560 Oceanography: Physical: Surface waves and tides (1255); *KEYWORDS:* ripples, waves, shelf, SHOWEX, observations, North Carolina.

Citation: Ardhuin, F., T. G. Drake, and T. H. C. Herbers, Observations of wave-generated vortex ripples on the North Carolina continental shelf, *J. Geophys. Res.*, *107*(0), XXXX, doi:10.1029/2001JC000986, 2002.

1. Introduction

[2] Bed forms on the sandy sea floor are an important source of hydrodynamic roughness for waves and currents in the surf zone and on the inner shelf [*Zhukovets*, 1963; *Scott and Csanady*, 1979]. Bed forms have a strong impact on the transport of sediments, either as a result of their migration or because of their influence on the flow that shapes them. Their presence, formation, and evolution have been observed extensively in nearshore environments [e.g., *Hunt*, 1882; *Forel*, 1883; *Dingler*, 1974; *Vincent and Osborne*, 1993; *Gallagher et al.*, 1998; *Traykovski et al.*, 1999]. In the absence of mean currents, waves can generate ripples that are symmetric in cross section. The formation of such wave ripples was first investigated in the laboratory by *Darwin* [1883] using a rotating bath. He noted the important role of the vortices generated in the lee of the ripples, further observed by *Ayrton* [1910], eroding the ripple troughs and building up the crests. Such bed forms, termed "vortex ripples" by *Bagnold* [1946], exert a much larger drag on the flow than friction on sand grains. Vortex ripples occasionally have been called "orbital ripples" because their wavelength is related to the near-bed orbital diameter of the wave motion, or "megaripples" when they exceed some large wavelength, although they should not be confused with nearshore short-crested megaripples generated by different processes [*Gallagher et al.*, 1998].

[3] Based on dimensional analysis and numerical morphodynamic modeling, *Andersen* [1999] and *Andersen and Fredsøe* [1999] found that the wave flow over ripples is essentially governed by two nondimensional parameters, λ/d and η/λ, where λ and η are the ripple wavelength and height and d is the diameter of the bottom orbital excursion of water parcels. Sediment motions are governed by two additional parameters, the ratio $w_s/u_{\max}$ of the settling velocity of sand grains w_s and the maximum near-bed orbital velocity $u_{\max}$ and the maximum ratio of friction and buoyant forces acting on a sand grain, represented by the Shields number $\psi_{\max}$ (often denoted $\theta'_{\max}$)

$$\psi_{\max} = \frac{f'_w u^2_{\max}}{2(s-1)gD}, \quad (1)$$

0148-0227/02/2001JC000986$09.00

where f'_w is a skin friction factor, s is the specific density of the sand grains, D is the grain diameter, and g is the acceleration of gravity [*Shields*, 1936]. When $\psi_{\max}$ is larger than a critical value ψ_c, the flow is able to move sand grains. If the bed is initially flat, "rolling-grain ripples" will form as a result of an instability. Each grain creates a region of weaker flow ("shadow") in its lee, and grains tend to group and form ripples with larger shadows [*Blondeaux*, 1990; *Vittori and Blondeaux*, 1990; *Andersen*, 1999]. These rolling-grain ripples eventually evolve into vortex ripples [*Sherer et al.*, 1999; *Faraci and Foti*, 2001]. The height η of vortex ripples is generally closely related to λ. The ripples are steepest for $1 < \psi_{\max}/\psi_c < 4$, when the vortices created in the lee of the crests maintain η/λ values between 0.1 and 0.2 [*Nielsen*, 1981]. For very large values of $\psi_{\max}$ of the order of $10\psi_c$ [*Li and Amos*, 1999], a layer of sediment (the "sheet flow") moves with the water column, ripples are washed out, and the dissipation of wave energy in the bottom boundary layer is relatively weaker.

[4] Numerical model simulations of the morphodynamics of one-dimensional ripples under sinusoidal waves confirm that the vortex forming in the lee of the crest with a size of the order of the orbital diameter d exerts a strong shear on the lee-side slope of the ripples that tends to build up the crests together with the flow on the upstream slope of the ripple [*Andersen*, 1999]. If two ripples are initially closer than a minimal stable wavelength λ_m, the vortex in the lee of the upstream ripple will erode the downstream ripple and one ripple may disappear creating a default in the regular spacing of the bed that will allow λ to grow. Conversely, ripples that initially are much further apart than λ_m will promote the generation of ripples in the troughs, dividing λ by a factor of 2. Values of λ_m were found to be related to the orbital diameter with $\lambda_m = 0.4d$ when $w_s/u_{\max} < 0.07$, and $\lambda_m = 0.63d$ when $w_s/u_{\max} > 0.07$. The transition for $w_s/u_{\max} = 0.07$ corresponds to a shift in the principal mode of sediment transport from suspended load to bed load, and the evolution from two-dimensional to three-dimensional ripple patterns [*Nielsen*, 1979]. In this context of decreasing orbital motion amplitude, the movement of defects in the three-dimensional ripple pattern should tend to reduce the average crest distance to λ_m [*Andersen and Fredsøe*, 1999]. Other classifications and characterizations of wave-generated ripples have been proposed based on empirical evidence [e.g., *Mogridge et al.*, 1994; *Wiberg and Harris*, 1994], but they failed to reconcile all laboratory and field observations.

[5] On a natural sea bed, ripples may be further affected by the presence of wave groups [e.g., *Madsen et al.*, 1990], the mixture of grain sizes [e.g. *Wallbridge et al.*, 1999], and the directional distribution of the waves [*Willis et al.*, 1993], although experiments support simple parameterizations using "equivalent parameters", e.g., median grain size D_{50}, velocity $u_{1/3}$, orbital diameter $d_{1/3}$, and Shields number $\psi_{1/3}$ based on the significant wave height $H_{1/3}$ [e.g., *Traykovski et al.*, 1999].

[6] Here observations of surficial sediments and wave-generated ripples, across the North Carolina continental shelf, are presented. The analysis is motivated by observations [*Herbers et al.*, 2000; *Ardhuin*, 2001] and numerical modeling studies [*Ardhuin et al.*, 2001] of strong damping of swell propagating across the shelf. Although the damping was consistent with a parameterization of the drag induced by wave-generated vortex ripples (see *Tolman* [1994], based on theoretical and experimental results of *Grant and Madsen* [1979] and *Madsen et al.* [1990]), no seabed data was available to verify the presence and properties of bed forms. The new data (section 2) include sediment samples, repeat side-scan sonar images of the bottom, and 3-month-long observations of wave frequency directional spectra. The analysis of sediment data and side-scan sonar images, giving the direction and wavelength of ripples, are presented and compared with previously reported data (sections 3 and 4). Observed ripple properties and preceding wave forcing conditions are compared in section 5 with the parameterization of *Andersen and Fredsøe* [1999] and the observations of *Traykovski et al.* [1999]. A discussion and summary are given in section 6.

2. Experiment

[7] Wave, bed form, and sediment data were collected off the coast of Duck, North Carolina, from September to December 1999, as part of the Shoaling Waves Experiment (SHOWEX) a multi-institution effort to improve the understanding of the transformation of waves in shallow water. The experiment site is a wide sandy continental shelf, exposed to North Atlantic swells. The bottom slopes gently from 20 m depth, 5 km from shore, to 40 m depth, over a distance of 60 km (Figure 1) and is characterized by the presence of sand ridges with spacings and heights ranging from ~1 to 10 km and 1–10 m, respectively [*Green*, 1986; *Wright*, 1995; *Ardhuin and Herbers*, 2001]. The larger-scale ridges are oriented along a south-north axis (Figure 1).

[8] Six Datawell directional wave rider buoys, named X1 through X6, were deployed from 13 September to 13 December 1999, along a cross-shelf transect. Buoys X1 through X5 span the shelf from 21 to 39 m depth, and buoy X6 was located on the shelf break in 193 m depth. Wave frequency spectra and directional moments (mean propagation direction and directional spread) as functions of frequency were computed internally by the buoys at 30-min intervals and transmitted continuously to shore by buoys X1 to X4 using HF radio. Buoys X5 and X6, situated farther offshore, were equipped with internal data loggers. The significant wave height $H_{1/3}$ (4 times the root-mean-square surface displacement) and spectral peak frequency f_p observed at X1 and X3 are shown in Figure 2 for energetic periods preceding three cruises when side-scan sonar images of the bottom were acquired. Figure 2 also displays the mean wave direction $\theta_E(f)$, defined as the direction of the first moment vector of the frequency directional surface elevation spectrum $E(f,\theta)$

$$[a_1(f), b_1(f)] = \int_0^{2\pi} (\cos\theta, \sin\theta) E(f,\theta) \mathrm{d}\theta. \qquad (2)$$

The large long-period waves (peak frequencies ranging from 0.06 to 0.08 Hz) originated from three category 4 hurricanes: Dennis looped offshore of the buoy transect (29 August to 5 September) before coming ashore farther south; Floyd swept through the region, with the eye passing a few tens of kilometers inland on 15 September; and Gert

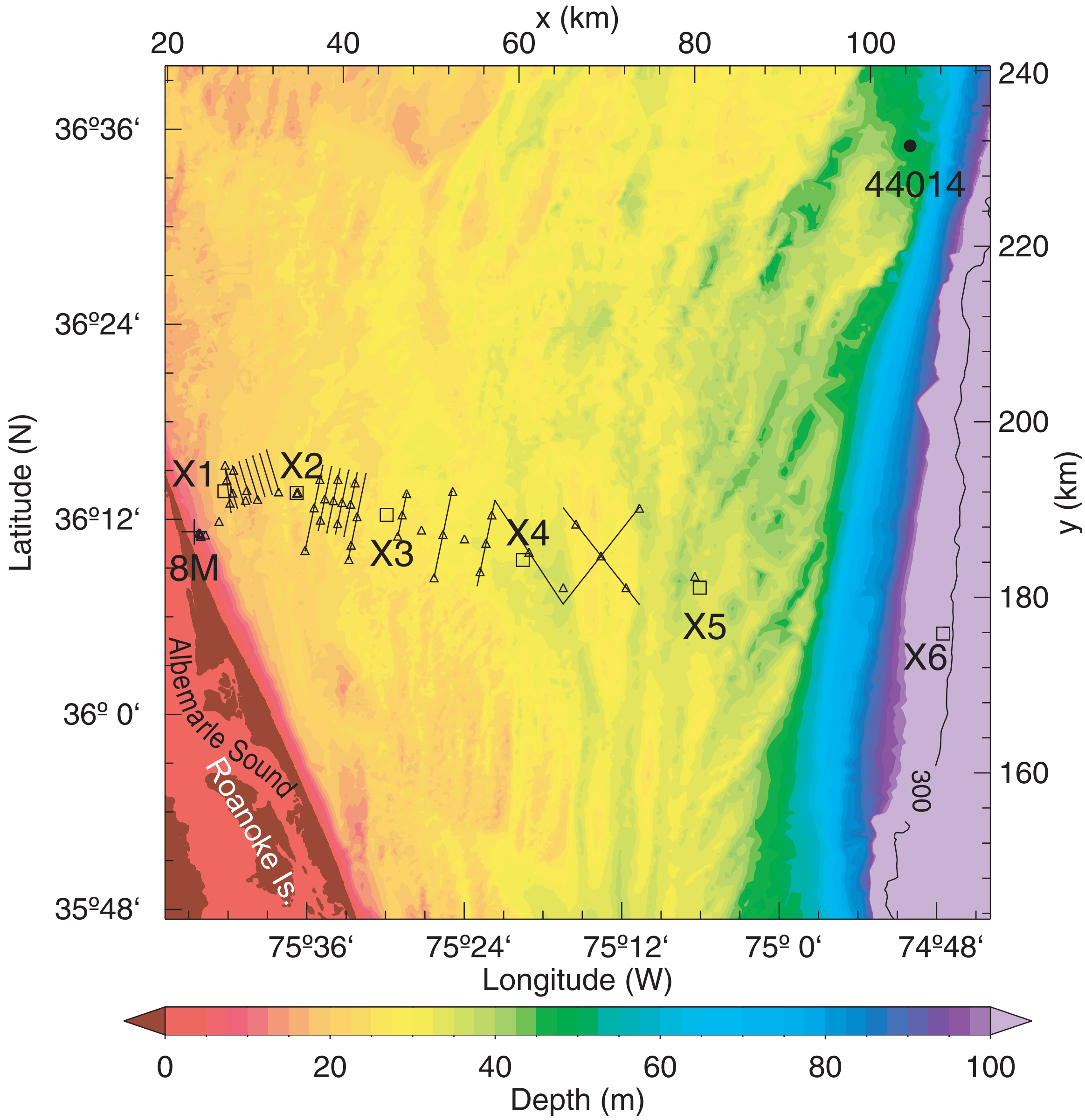

Figure 1. Bottom topography of the continental shelf off Duck, North Carolina. Squares numbered X1–X6 indicate the positions of directional wave rider buoys deployed during Shoaling Waves Experiment (SHOWEX), the solid circle indicates the National Data Buoy Center buoy 44014, and the plus indicates the field research facility 8 m depth pressure sensor array (8M). Solid lines represent ship tracks for the side-scan sonar surveys, and triangles indicate the locations where surficial sediments were sampled.

remained more than 1200 km away from the experiment site, sending swell along the buoy transect (20–23 September). The month of December was marked by a strong northeaster (1 and 2 December). The observed strong attenuation of wave energy between X3 and X1, particularly for low-frequency waves when $H_{1/3}$ was in the range 1–2 m, is consistent with previous observations and the large bottom roughness predicted for wave-formed ripples [*Herbers et al.*, 2000; *Ardhuin et al.*, 2001].

[9] Bed forms were surveyed with an EG&G model DF1000 side-scan sonar, towed from the R/V *Cape Hatteras* at night during cruises for buoy deployment, maintenance, and recovery. The first survey (S1) took place between the passages of hurricanes Dennis and Floyd from 10 to 13 September. A second survey (S2) was conducted 2 weeks later (24–26 September) after swells from Gert and a coincident northeasterly wind sea had subsided. Repeating most of the tracks from survey S1, the objective of S2 was an assessment of changes in bed forms after hurricanes Floyd and Gert. The final survey (S3) took place as buoys were being recovered (12–15 December) after a series of northeasters. The same tracks were repeated again, and a few additional regions were surveyed (all ship survey tracks for S3 are shown in Figure 1).

[10] The dual frequency sonar (100 and 500 kHz), was towed 2–3 m above the bottom in the shallower regions and

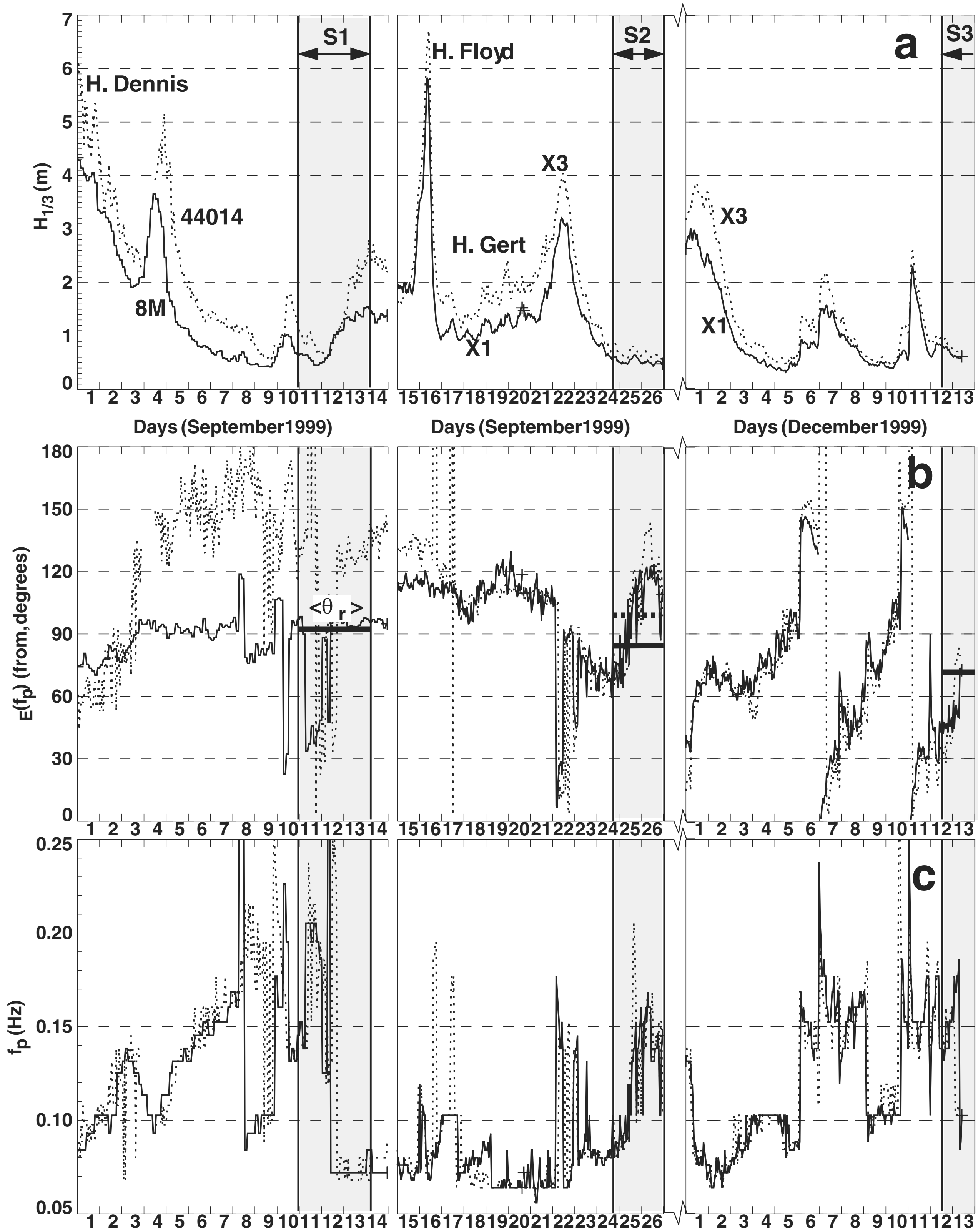

Figure 2. (a) Evolution of significant wave height $H_{1/3}$. (b) Mean wave direction at the peak frequency $\theta_E(f_p)$. (c) Peak frequency f_p. Observations are shown at buoys X1 (solid) and X3 (dotted), spanning the inner shelf. Before survey S1 (conducted during the buoy deployment cruise), data from 8M and 44014 are shown. During Hurricane Dennis, $\theta_E(f_p)$ at X1 is estimated to be $0°-10°$ larger than $\theta_E(f_p)$ measured at 8M, owing to refraction. For each survey the average of crest-normal ripple directions θ_r observed in the vicinity of X1 is indicated with a solid horizontal bar. The dashed bar indicates the more southerly average θ_r of ripples observed close to X3 during survey S2.

10–15 m in regions deeper than 30 m at a speed of ~2.3 m s^{-1}. The 100 kHz frequency was used throughout for larger area coverage at the expense of poorer resolution. All backscatter sonograms, covering a 100-m wide swath along a total track length of 420 km, were both recorded in a digital format and printed on paper scrolls. In selected regions where ripples were clearly visible the digital data was transformed into GEO-TIFF mosaics, fully corrected for slant range and speed, with a resolution of 5 or 10 pixels per meter. Surficial sediments were collected with a Shipek grab (46 samples), and by divers (5 samples), at locations indicated in Figure 1.

3. Surficial Sediments

[11] The continental shelf between Cape Hatteras and the entrance to the Chesapeake Bay (Cape Henry) is believed to be covered by fine quartz sand [*Milliman et al.*, 1972; *Swift and Sears*, 1974], with occasional coarser sands and gravel in fluvial paleochannels flooded by Holocene sea-level rise [*Swift et al.*, 1972]. The Albemarle River paleochannel coincides with the buoy transect (Figure 1). Very fine sands with a silt and clay content of 10–26% are found between 8 and 18 m depth [*Field et al.*, 1979; *Wright*, 1993; *Madsen et al.*, 1993], and their origin can be traced to old lagoonal deposits [*Wright*, 1995].

[12] The samples gathered during the three cruises confirm this pattern. Most samples consisted of fine sand with a median diameter D_{50} of ~0.2 mm (Figure 3). Samples occasionally contained shell hash, particularly around X1 (Figure 1). Grain sizes at neighboring sample sites can be significantly different, suggesting strong variability of sediment properties on scales less than a few kilometers, in particular, on the inner shelf between X1 and X2 (Figure 4a). For example, the finest sand (D_{50} = 0.09 mm, asterisks in Figure 3) was found in 12 m depth, and the coarsest sample, a mixture of sand and small gravel with D_{50} = 4 mm (triangles in Figure 3), was found in the vicinity of X1, in 19 m depth. All samples taken near X2 were fine sand, except for one coarse sample collected by divers within 300 m of X2 that contained pebbles several centimeters in diameter, that could not be analyzed quantitatively.

[13] The variability of sediment properties also is evident in the side-scan sonograms. For the range of grain sizes found in the samples, a stronger reflectivity (dark shades in the sonograms) usually corresponds to coarser sands. A large portion of the regions surveyed between X1 and X2 show alternating light and dark bands (the coarsest sand found in the samples came from one of these dark bands) a few hundred meters wide, with sharp transitions. Offshore of X2, some dark bands are still present, although they contrast less with their lighter surroundings. This alternating pattern is similar to the one found by *Green* [1986] in a side-scan sonar survey conducted in 1984, 6 km south of X1. *Green* [1986] identified dark bands lying in the troughs between ridges oriented north-south (with approximate heights and spacings of 5 and 500 m, respectively) as the pre-Holocene "basement" underlying the finer Holocene sand ridges. In the surveys presented here the dark regions also correspond to relatively low-lying areas, at least inshore of X3 where high-resolution multibeam sonar surveys were conducted in December 1999 [*Ardhuin and Herbers*, 2001].

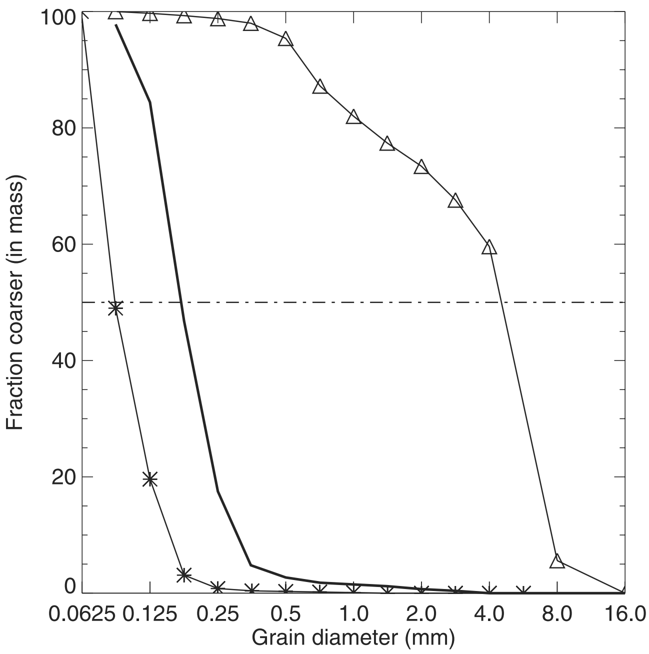

Figure 3. Example grain size distributions. A typical distribution (thick solid line) and the distributions with the finest (asterisks) and coarsest (triangles) sediments are shown.

4. Side-Scan Sonar Images of Bed Forms

[14] In addition to qualitative information on sediment grain sizes the side-scan sonar images document the occurrence and characteristics of bed form patterns. A qualitative inspection of the entire sonar data set for the three surveys (Figures 4b–4d) reveals the predominance of symmetric, long-crested ripples with wavelengths between 0.4 and 3 m and crests approximately parallel to the coastline, consistent with the scales and orientation of vortex ripples formed by large low-frequency surface gravity waves propagating across the shelf. Hummock-like ripples, characteristic of combined wave-current flows [e.g., *Li and Amos*, 1999], were occasionally seen (they cover ¡1% of the surveyed area) and may have been formed at times when currents were relatively important. However, the observed predominant symmetric long-crested ripples are characteristic of wave-dominated flows. Mean currents were therefore probably weak during the formation of these ripples, an assumption consistent with previous measurements at the same site that show weak tidal currents [*Lentz et al.*, 1999], and mean wind-driven currents speeds are typically less than half the root-mean-square of wave-induced velocities in both calm and storm conditions [*Madsen et al.*, 1993; *Lentz et al.*, 2001].

[15] In cross-shore surveys, ripple marks are faint or absent, probably because the alongshore orientation of the sonar beams (perpendicular to the ship track) was at a grazing angle relative to the ripple crests, usually oriented alongshore. Images from part of the surveys were blurred by excessive wave-induced tow-fish motion. In regions where ripples were not detected the bottom may be smooth as a

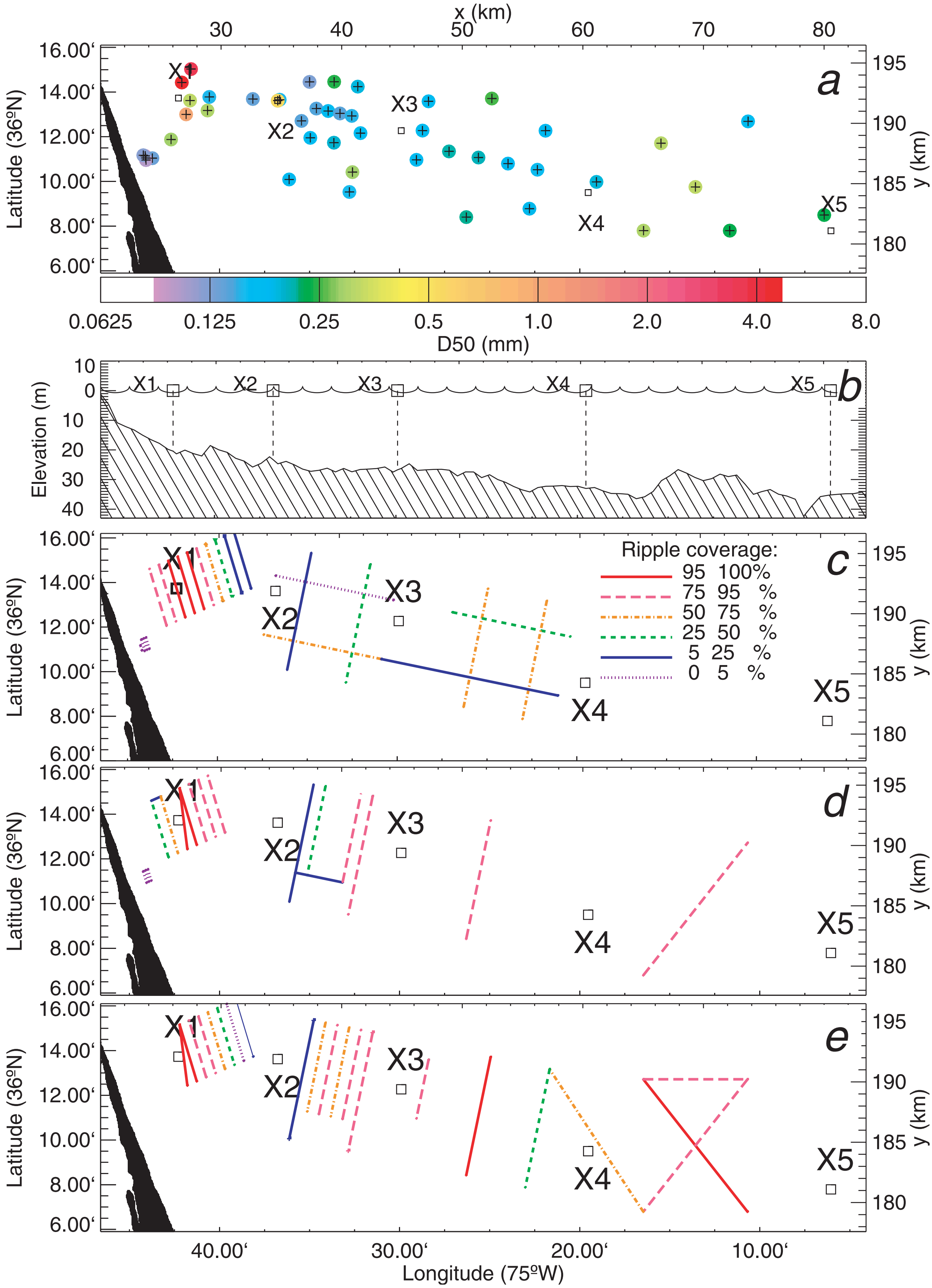

Figure 4. (a) Geographical distribution of the median grain size D_{50}. (b) Depth profile along the X1–X5 transect. (c–e) Fraction of sonar surveyed regions visibly covered by ripples for surveys S1, S2, and S3, respectively.

result of the possibly shallow nature of the sediment cover or some other unknown phenomenon, but ripples may be present and too small to be resolved. For example, at a site in 12 m depth in fine sediments (D_{50} = 0.09 mm, asterisks in Figure 3), high-resolution mapping instruments located on an bottom-mounted frame showed the presence of short wavelength (10–20 cm) ripples not resolved in our surveys (T. P. Stanton, personal communication, 2000). The absence of ripples in alongshore ship tracks usually corresponds to regions with finer surficial sediments. Assuming that vortex ripples, for which the wavelength scales with the near-bed wave orbital diameter, are formed by wave action during a storm and become relic when the near-bed velocity decreases, ripples formed in finer sand are "frozen" later, when the waves are smaller, and thus are expected to have shorter wavelengths (i.e., not resolved by the sonar) than ripples in coarse sand.

[16] A quantitative analysis was performed for surveyed regions with clearly visible bed forms and relatively uniform bed form geometry, and sound reflectivity. For each region a representative 100 m by 100 m image was processed. In some cases with faint ripples a smaller image with clear ripple crests was analyzed. Although spectral analysis is well suited to characterize regular ripples, bidimensional variance spectra computed from sonar images exhibit multiple peaks in many cases, either as the result of excessive side-scan towfish motions (along-track modulations of ripple patterns on the sonar images) or because of the presence of many defects in the ripple patterns. Consequently, a procedure that is less sensitive to defects and image artifacts was used (Figure 5). For each image, after subtracting a piecewise bilinear fit to the pixel values, we computed the zero-crossing contours of the image intensity and formed a histogram of the contour length as a function of its orientation, at 1° intervals, using the trigonometric (right-handed) convention. A function $p(\theta) = a_0 + a_2 \cos[2(\theta - \theta_c)]$ was fitted to this histogram in a least-squares sense, and θ_c was interpreted as the mean orientation of the ripple crests. The ratio a_2/a_0 gives an indication of the presence, long-crestedness, and regularity of ripples. For high contrast ripples with long crests and few pattern defects, $a_2/a_0 > 1$ (e.g., Figures 5a and 5b). For faint ripples or ripples with short or brick-patterned crests, $a_2/a_0 < 0.5$. An example of marginally detectable and nonuniform ripples, with a_2/a_0 = 0.8, in shown in Figure 5c. Once θ_c was determined, standard one-dimensional Fourier spectra were computed for east-west image lines (usually within 30° of the crest-normal direction). The spectra were then averaged over all lines, and the peak wave number k_p was determined. The average wavelength of the ripples λ was then taken to be $2\pi \sin \theta_c / k_p$, and the crest-normal direction, using the (left-handed) nautical convention, was given by $\theta_r = 180(1-\theta_c/\pi)$. In cases with $a_2/a_0 < 0.4$ this procedure failed to determine θ_r and λ unambiguously, and the bed was presumed featureless.

[17] In most images with visible ripples the dominant bed forms are regular long-crested ripples (Figure 5). Spatial variations observed in the backscatter sonar intensity and ripple patterns are the result of nonuniformities in sediment properties (e.g., variations in grain size, Figure 6a) or small-scale (unresolved) ripples or both. A few regions reveal intricate bed form patterns with double crests or secondary small crests in the troughs of larger ripples (Figure 6b) that may be the result of decreasing wave-forcing conditions. Earlier observations and numerical modeling studies have shown that when the mean wave direction is constant, ripple wavelengths gradually increase with increasing wave orbital diameter $d_{1/3}$, but the converse is not true, and thus when $d_{1/3}$ decreases, the ripple wavelengths typically remain unchanged. For decreasing $d_{1/3}$, if the Shields number threshold for sediment motion is still exceeded, secondary ripple crests may appear in the troughs, reducing the wavelength by half [*Forel*, 1998; *Traykovski et al.*, 1999; *Andersen*, 1999]. Other ripple patterns include superpositions of two ripple systems (e.g., Figures 6c and 6d) similar to previous observations [e.g., *Forel*, 1998; *Swift et al.*, 1972]. As discussed below, these patterns likely are caused by successive wave events with different wave directions. The wavelengths in some of these ripple systems can be as large as 4 m, of the order of the wavelengths of long-crested features observed in this region and called "megaripples" by *Green* [1986]. The variety of observed bed form patterns underscores the important effects of past bed form evolution on their present state in the relatively mild forcing conditions prevalent during these surveys.

[18] Temporal changes in ripple direction θ_r and wavelength λ are examined in Figure 7 using repeated survey track lines close to X1. All surveys reveal widespread ripple coverage with typical wavelengths λ of 0.5–3 m, and ripple crest-normal directions θ_r between 60° and 120° (shore-normal is 70°). Changes observed between surveys S1 and S2 (Figures 7a and 7b) are small, with a slight shift of the average value of θ_r from 91° to 85°. A larger change in ripple orientation is observed in S3 with an average θ_r of 73° (Figure 7c).

[19] This observed change in bed forms is related to a change in wave conditions, from hurricane-generated waves from east to south-east propagation directions in September to northeasterly waves in December. The average values of θ_r in surveys S1, S2, and S3 (indicated by thick horizontal bars in Figure 2) correspond to the wave directions of preceding large wave events on 4–5 September (Hurricane Dennis), 22–23 September (Hurricane Gert), and 1–2 December (northeaster), respectively, suggesting that the observed ripples were formed in these periods. The large oblique ripples observed in S2 (λ = 2.0 m, θ_r = 105°) and S3 (λ = 2.0 m, θ_r = 132°) close to the northern end of the surveyed region are notable exceptions. The corresponding side-scan image of the anomalous ripples in S2, shown in Figure 6c, indicates that the estimated λ and θ_r are averages of two superposed ripple systems, λ = 2.0 m, θ_r = 120°, probably generated during the passage of Hurricane Floyd, and λ = 0.8 m, θ_r = 85°, probably generated during the arrival of swell from Hurricane Gert. Within 200 m of these ripples a similar but smaller patch of large ripples was observed in survey S3 (Figure 7c) with a more oblique angle θ_r = 132° that does not match the wave directions of any energetic wave event observed during the 3 months between surveys S2 and S3 that would be capable of moving bottom sediments in that region, suggesting that these ripples also were formed during Floyd and persisted throughout the experiment.

[20] Spatial variations in θ_r and λ across the shelf during survey S2 are shown in Figure 8. Observations on the middle and outer shelf show more southerly θ_r angles than observations on the inner shelf (Figures 8a–8c). Some spatial

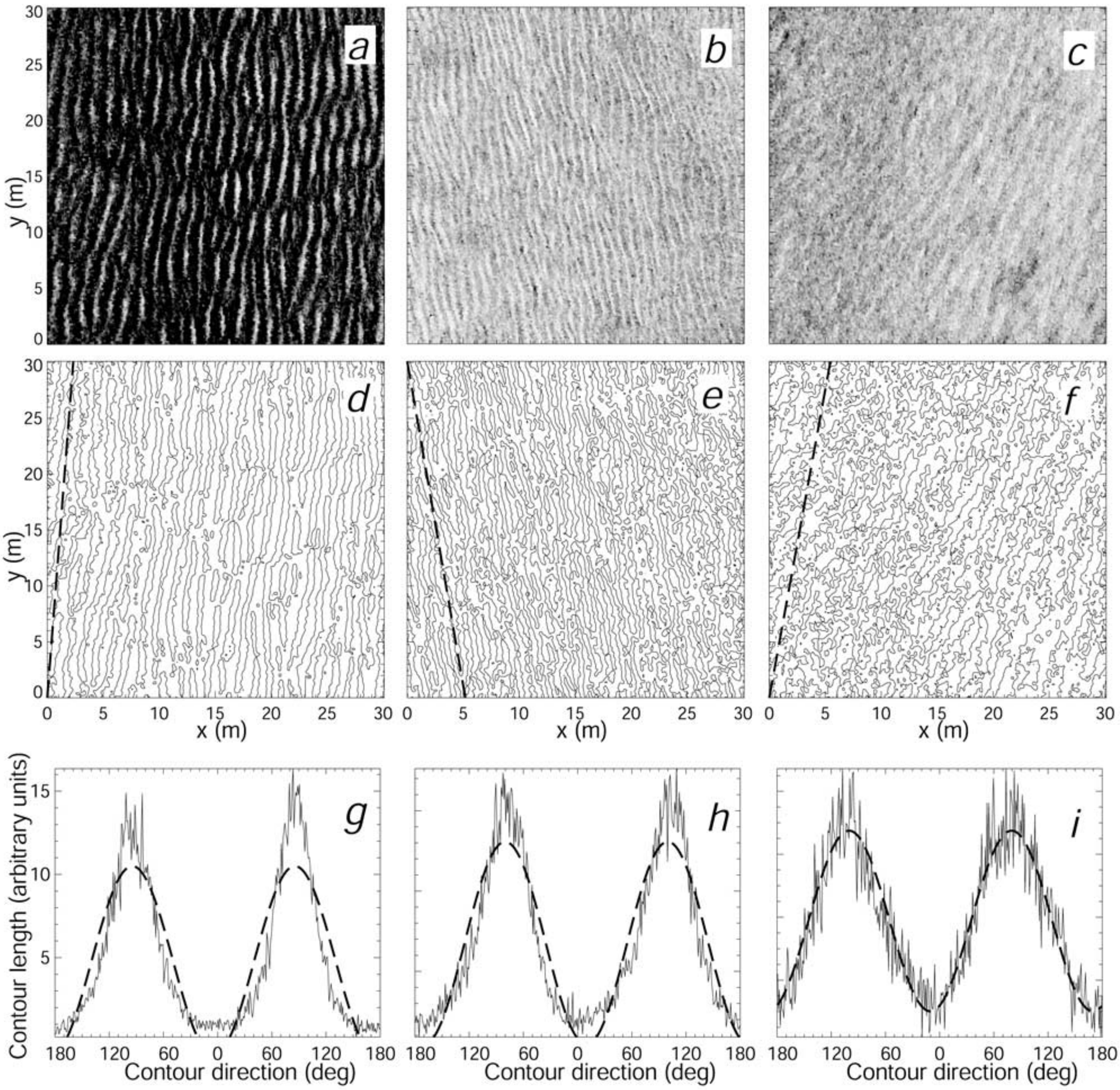

Figure 5. Extraction of ripple parameters from side-scan images. (a–c) Example images from the sites where samples 111, 114, and 207 were collected (see Table 1). (d–f) Corresponding zero-crossing contours with an indication of the mean crest orientation θ_c (dashed line). (g–i) Histogram of contour direction with fitted cosine distribution (dashed line).

variation of ripple directions is expected associated with the refraction of the swell that probably generated the bed forms. However, observed differences in wave direction θ_E between X3 and X1 are small compared with the 15° difference between the average θ_r around X3 and X1. Temporal changes of the wave-forcing conditions also may have contributed to these θ_r variations. In deeper regions where the wave motion is more attenuated over the water column, ripples may have become relic at an earlier stage when the swell was more energetic and arrived from a more southerly angle (Figures 2a and 2b). Indeed, the average θ_r values of 100° and 85° near X3 and X1, respectively (dashed and solid horizontal bars in Figure 2b) are close to mean wave directions on 22 and 23 September, respectively. Large variations of θ_r and λ also are observed over much shorter distances, with estimates varying by as much as 30° and a factor 2, respectively, within 1 km. These differences (Figures 8b and 8c) are caused primarily by the superposition of ripple patterns, some of which are barely resolved in our images. The relation between observed ripple geometry and changing wave forcing conditions is analyzed in section 5.

5. Evaluation of Ripple Parameterizations

[21] Bed forms observed in the sonar images usually are not related to the instantaneous wave forcing (surveys were

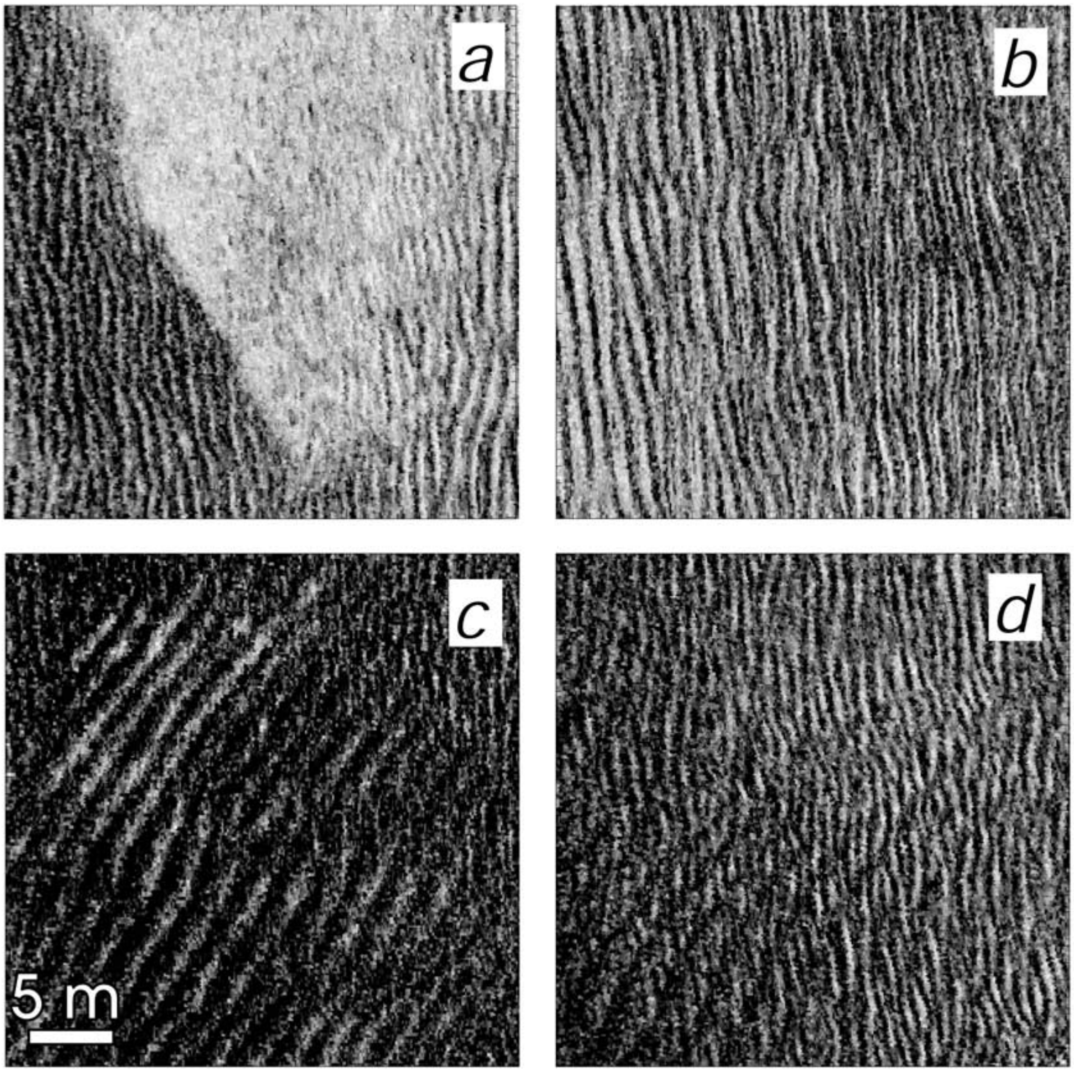

Figure 6. Examples of unusual ripple patterns. (a) Sharp transition in sediment properties. (b) Secondary ripples. (c and d) Superposition of ripple patterns (see section 4).

performed in relatively calm conditions) but are the result of earlier wave events that were sufficiently energetic to move the sediments. Here the ripple properties observed in surveys S2 and S3 are compared to the wave forcing history recorded at the nearest buoy. Neglecting variations in the wave forcing conditions over the 1–5 km distance separating the locations of the wave and ripple measurements, we computed a "significant" Shields number $\psi_{1/3}$ from equation (1) using a range of D_{50} values for the grain size and $u_{1/3}$ defined as 2 times the root-mean-square velocity near the sea bed, determined from the surface elevation frequency spectrum with linear wave theory. The skin friction factor f'_w was obtained with *Grant and Madsen*'s [1979, 1982] parameterization, based on a linear profile of the eddy viscosity (see also the review by *Tolman* [1994]). We assumed a threshold of ripple formation $\psi_{1/3} = \psi_c$ [*Traykovski et al.*, 1999], where ψ_c is the threshold of sediment motion under sinusoidal waves. *Madsen and Grant* [1976] give a review of values of ψ_c determined experimentally for well-sorted sand. Here we use a piecewise fit to the experimental data of *Wallbridge et al.* [1999] for mixed sands under combined wave-current flow that we apply to the median grain size,

$$\psi_c = 0.1 \exp\left[(S_* - 2)\ln(0.35)/10\right] \quad \text{for} \quad 2 < S_* < 12 \tag{3}$$

$$S_* = D_{50}\left[(s-1)gD_{50}\right]^{\frac{1}{2}}/(4\nu), \tag{4}$$

where ν is the kinematic viscosity of water. These values of ψ_c are slightly larger than those given by *Shields* [1936] or *Soulsby and Whitehouse* [1997] for unidirectional and combined wave-current flows ($\sim$30% larger in the range $3 < S_* < 12$) but follow the same trend, decreasing with increasing grain size. Based on these assumptions all but the coarsest surficial sediments have moved on 22 September and during the 1–2 December northeaster, after which ripples became relic and remained unchanged until surveys S2 and S3, respectively (Figure 9a).

[22] The interpretation of survey S2 is complicated by cross seas observed on 22 September (when the wave height was maximum) as different definitions of a representative

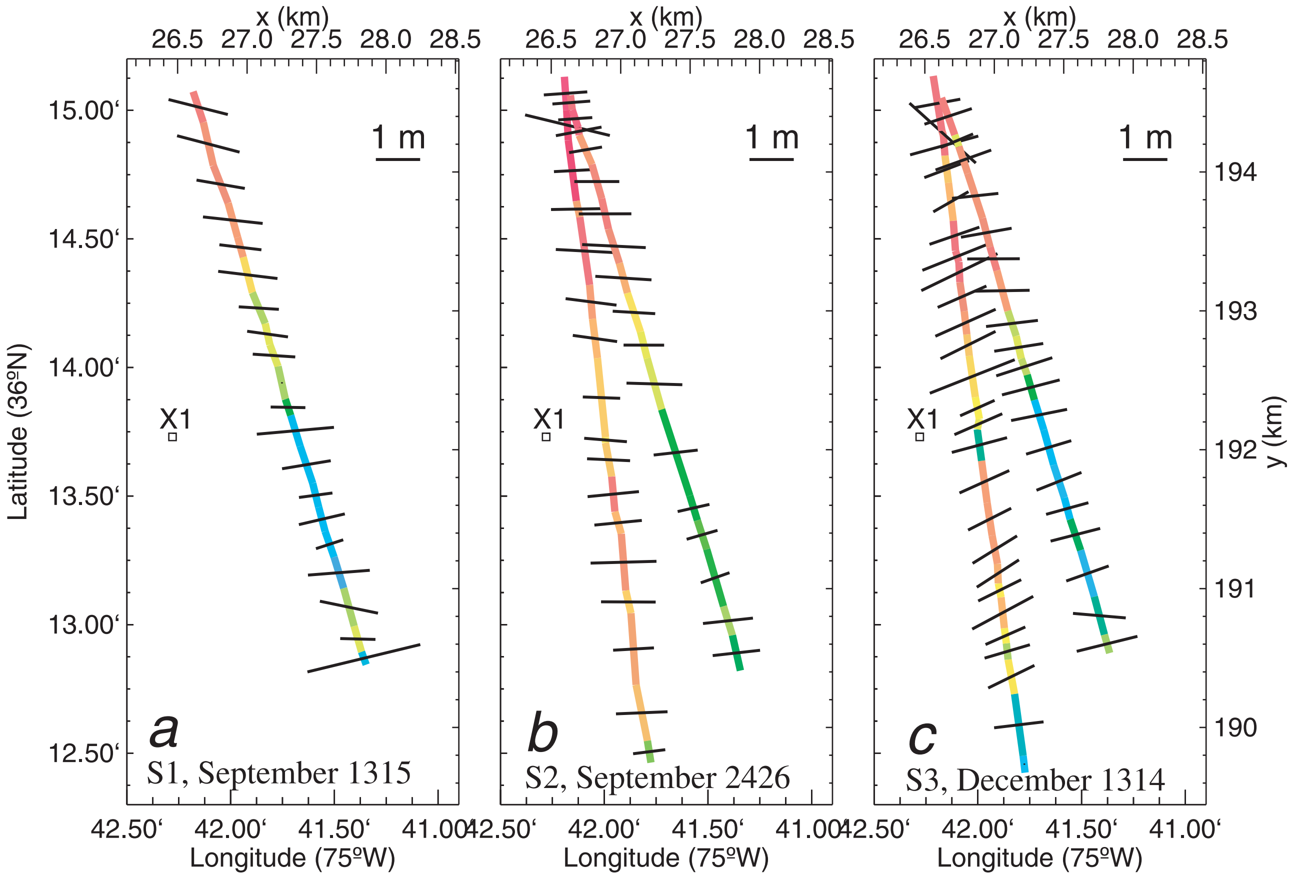

Figure 7. Distribution of ripple direction and wavelength for surveys (a) S1, (b) S2, and (c) S3. The thick bars indicate the crest-normal ripple direction θ_r, and the ripple wavelength λ with a scale is given in the upper right corner of each panel. Each bar is drawn in the middle of the survey segment for which the ripple parameters are representative. The colors along the survey line indicate the average backscatter strength of the side-scan sonar images. Red is strong (generally, coarse sand), and blue is weak (generally, very fine sand). Surveyed regions without a bar indicate the absence of ripples or a failure of the analysis procedure to determine θ_r and λ.

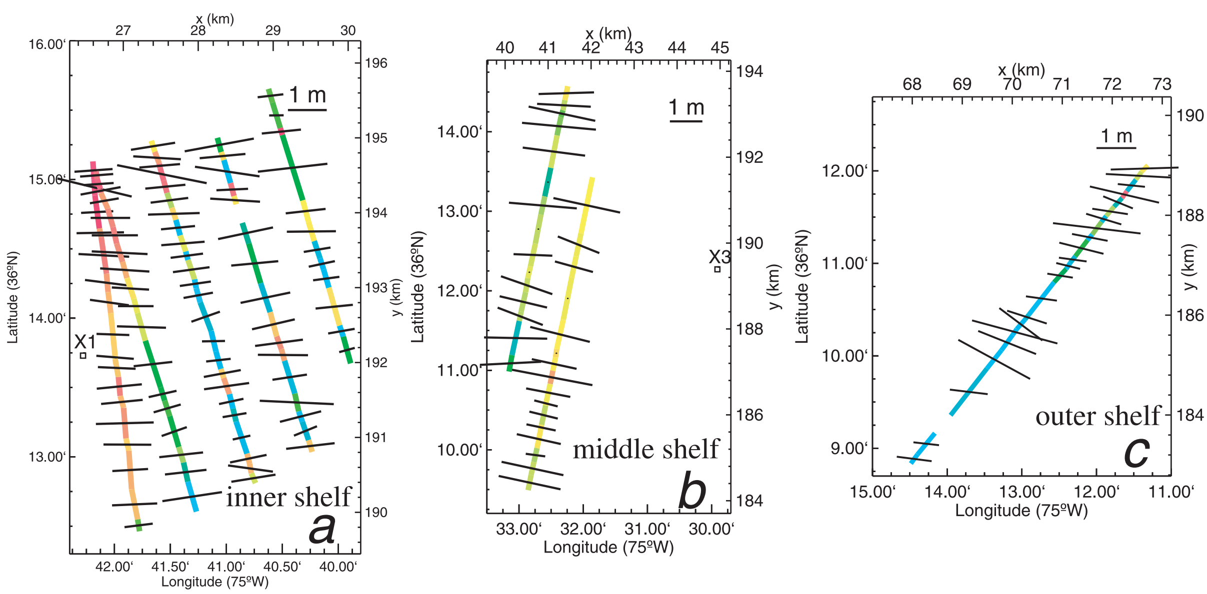

Figure 8. Same as Figure 7, for survey S2 only, at different locations across the shelf.

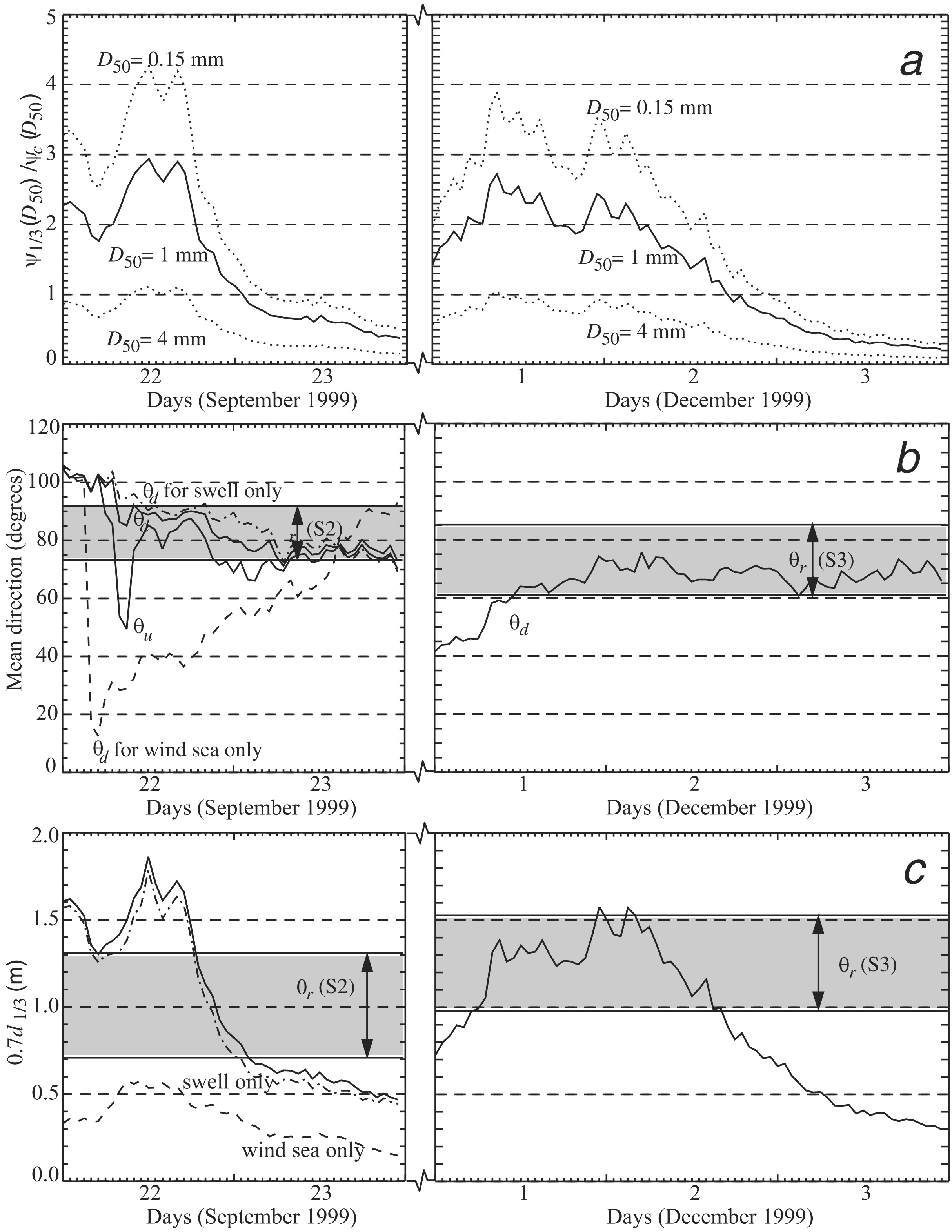

Figure 9. Wave-forcing conditions during ripple formation. (a) Values $\psi_{1/3}/\psi_c$ computed at X1 using the full wave spectrum and various values of the median grain size D_{50}. (b) Corresponding values of the mean direction of the orbital displacements at the top of the wave bottom boundary layer θ_d. For the complex 22–23 September wave conditions the mean direction of the near-bed orbital velocity θ_u, estimates of θ_d for swell (0.05–0.11 Hz), and wind sea (0.11–0.25 Hz) only are also indicated. (c) Corresponding values of predicted ripple wavelength $0.7d_{1/3}$ for vortex ripples, where $d_{1/3}$ is the significant diameter of the orbital displacement at the top of the wave bottom boundary layer. The grey bands in Figures 9b and 9c represent the mean value of the crest-normal ripple direction θ_r and wavelength λ, respectively, ±1 standard deviation, observed in the vicinity of X1 (Figures 7b and 7c).

wave forcing direction yield different ripple predictions depending on the relative importance given to motions with higher and lower frequencies. Here the bulk mean directions of the near-bed orbital velocity θ_u and displacement θ_d, are defined as the directions of the first spectral moment vectors

$$(a_u, b_u) = \int \frac{2\pi f}{\sin h^2(kH)} \int_0^{2\pi} (\cos\theta, \sin\theta)\, E(f, \theta)\, d\theta df \qquad (5)$$

$$(a_d, b_d) = \int \frac{1}{\sin h^2(kH)} \int_0^{2\pi} (\cos\theta, \sin\theta)\, E(f, \theta)\, d\theta df, \qquad (6)$$

where the angle θ is defined with the nautical convention. The superposition of a local wind sea traveling at right angles to swell from Hurricane Gert caused θ_u to veer to the north from 85° to 50° and then back to the east, whereas θ_d shifted gradually from 95° to 70° (Figure 9b). Although the high-frequency seas contributed significantly to the near-bed velocity variance and Shields number $\psi_{1/3}$ (equal contributions from the 0.05–0.11 and 0.11–0.25 Hz frequency ranges when $\psi_{1/3}$ is maximum), the orbital displacement direction θ_d remained aligned with the lower frequency swell. Observed ripple crest-normal directions θ_r are closer to θ_d than θ_u at possible freezing times ($\psi_{1/3} \simeq \psi_c$, Figure 9a). These observations suggest that the mean direction of the orbital displacement θ_d, which is less influenced by high-frequency (wind sea) motion, may describe better the relation between wave direction and ripple orientation (Figure 9b). The $\psi_{1/3} = \psi_c$ ripple freezing threshold yields values of θ_d that are still 5°–10° to the south of θ_r.

[23] Several factors may contribute to this difference. A re-orientation of the ripple pattern may require a larger forcing ($\psi_{1/3}$) than the initiation of sediment motion (ψ_c) [*Werner and Kocurek*, 1997], the time of adjustment of the bed forms in conditions close to the threshold may be larger than the timescale of the wave height decrease, θ_r may not be simply related to θ_d, or the values of ψ_c are not well predicted by equations (3) and (4). Such "early freezing" of ripples in conditions of decreasing forcing also was observed by *Traykovski et al.* [1999] with frozen bed form patterns for $\psi_{1/3}$ as large as $2\psi_c$. Although the exact threshold for the cessation of ripple evolution is uncertain, the observed wavelengths λ fall within the range of wavelengths expected for vortex ripples ($\lambda \approx 0.7d_{1/3}$, as observed by *Traykovski et al.* [1999]) when the Shields number $\psi_{1/3}$ dropped to values in the critical range 1–3 ψ_c (Figures 9a and 9c, using representative grain sizes), suggesting that the observed ripples were indeed of the "vortex ripple" type, similar to those observed by *Traykovski et al.* [1999].

[24] Analysis of bed forms at sites that coincide with the location of sediment samples shows that the ratio λ/D_{50} varies from 300 to 8100 (Table 1), extending the range of previously observed values [*Wiberg and Harris*, 1994] to more energetic forcing conditions. Crude estimates of active ripple forcing conditions can be obtained from the preceding wave records by determining the most recent time when ripples and wave crests were aligned (taking $|\theta_d - \theta_r| < 5°$), while surficial sediments were still in motion (assuming $\psi_{1/3} > 0.8\psi_c$). This analysis gives values of $\psi_{1/3}/\psi_c$ between 0.9 and 3.5 and values of $\lambda/d_{1/3}$ from 0.5 to 0.76 (Table 1).

Table 1. Ripples at Sites of Sediment Sample Collection[a]

	Sample							
	111	110	114	11	207	212	206	205
Nearest buoy	X1	X1	X1	X1	X3	X3	X3	X3
Depth, m	22.3	19.7	20.7	21.2	22.7	27.6	26.3	27.4
D_{50}, mm	4.71	0.98	0.32	0.15	0.28	0.19	0.17	0.15
D_{85}, mm	7.30	2.29	0.48	0.28	0.68	0.28	0.25	0.24
θ_r	94°	85°	80°	88°	101°	99°	NA	NA
λ, m	1.25	1.20	0.77	1.22	1.30	1.37	NA	NA
$d_{1/3}$, m	2.55	1.85	1.34	1.60	2.73	2.34	NA	NA
$u_{1/3}$, m s^{-1}	0.58	0.48	0.37	0.42	0.67	0.55	NA	NA
$\psi_{1/3}/\psi_c$	0.90	2.00	1.33	3.54	3.4	3.0	NA	NA
$w_s/u_{1/3}$	0.50	0.25	0.10	0.03	0.08	0.04	NA	NA
$\lambda/d_{1/3}$	0.49	0.65	0.58	0.76	0.48	0.59	NA	NA
$d_{1/3}/D_{50}$	540	1900	4200	10700	9800	12300	NA	NA
λ/D_{50}	270	1200	2400	8133	4600	7200	NA	NA

[a] The orbital diameter $d_{1/3}$ and corresponding velocity were determined by matching the bottom orbital displacement direction θ_d (computed from the frequency-directional wave spectrum at the nearest buoy and the local water depth) to the direction normal to the ripple crests θ_r (see section 5). No ripples were detected where samples 306 and 205 were collected. NA, not available.

Although these estimates have a large uncertainty and should be considered with caution, they are consistent with accurate measurements by *Traykovski et al.* [1999], who observed that λ is close to $0.76d_{1/3}$ under moderate forcing conditions. These estimates are also qualitatively consistent with the values of λ/d predicted by numerical simulations with sinusoidal waves [*Andersen*, 1999], although there is no strong increase of λ/d with the normalized fall velocity w_s/u.

[25] Estimates of ripple direction θ_r and wavelength λ in surveys S2 and S3 are summarized in Figure 10 for the region around X1. The observations in S2 show a clear trend of increasing wavelength corresponding to more southerly angles (Figure 10a). This trend is consistent with the freezing of the largest ripples shortly after the peak of the event (22 September) and a later freezing in finer sediments where the ripple patterns gradually adjusted to the more northerly angles and small orbital diameters of the waves observed on 23 September. Observations in S3 (Figure 10b) do not indicate a clear relation between θ_r and λ, possibly because the wave direction remained steady when the storm subsided on 2 December. However, with the exception of apparent "Floyd survivors" (θ_r = 132°, λ = 2 *m*), the longer ripples (λ > 1.5 m) in S3 consistently have crest-normal directions at large northerly angles (60° < θ_r < 75°), suggesting they became relic on 1 December and early 2 December when wave directions were similar, and the orbital diameter $d_{1/3}$ was maximum.

6. Summary and Discussion

[26] Widespread formation and evolution of sand ripples on the North Carolina continental shelf, observed in side-scan sonar surveys, were examined in relation to time series of directional wave measurements. Sediment samples confirm the ubiquitous presence of very fine to fine quartz-dominated sand with significant variability in the grain sizes over distances ¡1 km, in particular, in regions shallower than 25 m. Side-scan sonar surveys reveal the presence of ripples in most surveyed areas, with wavelengths between 0.5 and 3 m and crest-normal directions within 30° of the west-east axis. The apparent absence of any bed forms in some

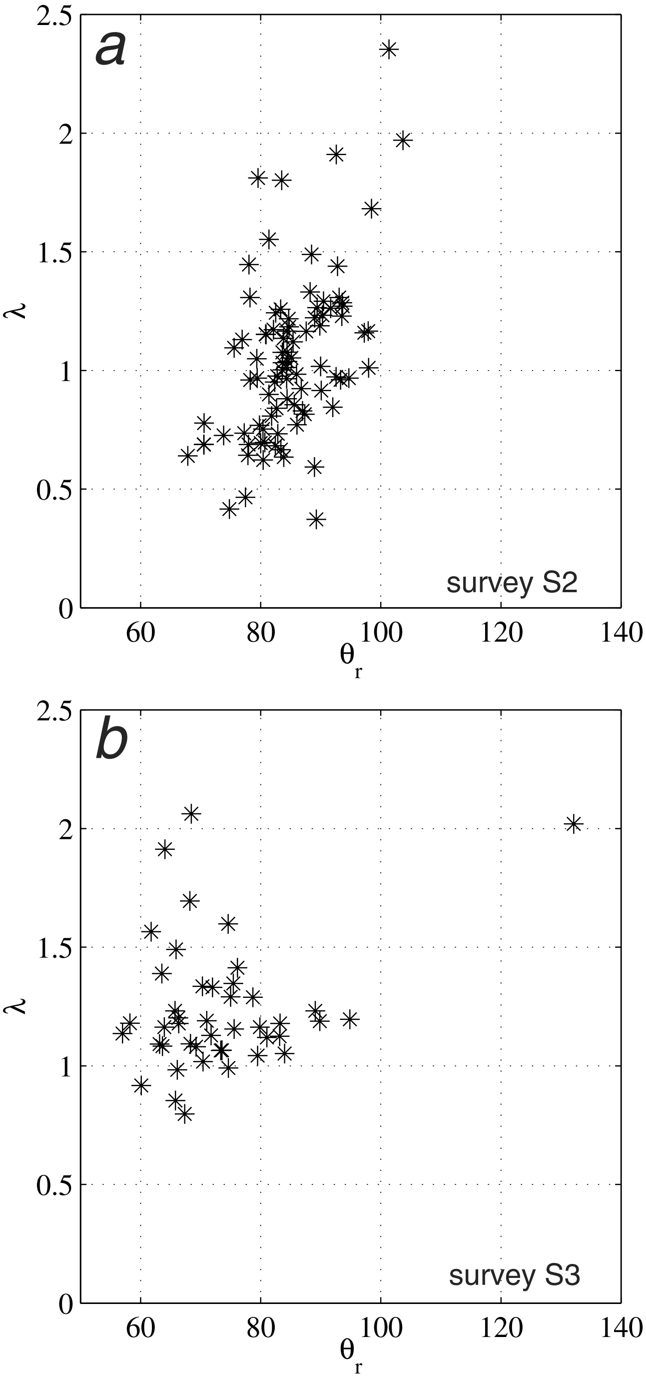

Figure 10. Ripple wavelength λ versus crest-normal ripple direction θ_r for ripples observed on the inner shelf in (a) survey S2 (Figure 8a) and (b) survey S3 (Figure 7c).

regions with finer sediments may be caused by their close spacing (¡40 cm) not resolved by the sonar images.

[27] The ripple crest-normal directions θ_r were aligned approximately with the direction of the near-bed orbital displacement θ_d when the ripples became relic. Although the precise time of cessation of sediment motion is uncertain, estimated ripple wavelengths λ and forcing conditions (the orbital diameter $d_{1/3}$) are consistent with previous observations of vortex ripples ($\lambda/d_{1/3} \simeq 0.5-0.76$) even for large values of $d_{1/3}/D_{50}$ and λ/D_{50}.

[28] The present data set extend the range of previous field observations of vortex ripples [e.g., *Traykovski et al.*, 1999] to larger adimensional orbital diameters $d_{1/3}/D_{50}$, but equally moderate Shields numbers $1 < \psi_{1/3}/\psi_c < 3$. Similar vortex ripples ($\lambda/d \approx 0.8$) have been observed for these large orbital diameters (d/D_{50} up to 2.5×10^4) in the laboratory [*Southard et al.*, 1990]. Both the present observations and these earlier laboratory and field studies do not support parameterizations of the ripples based on the grain size only [e.g., *Wiberg and Harris*, 1994] but imply a dependence of the ripple characteristics on the physical processes responsible for ripple formation, represented by the Shields number and possibly the sediment fall velocity, as represented in the parameterizations proposed by *Nielsen* [1981] and *Andersen and Fredse* [1999].

[29] The widespread presence of vortex ripples on the continental shelf lends support for a dominant role of these rough bed forms in the strong attenuation of swells observed in this and other coastal experiments, during periods of moderate to strong wave forcing when ripples should be generated [*Hasselmann et al.*, 1973; *Young and Gorman*, 1995; *Herbers et al.*, 2000; *Ardhuin et al.*, 2001; *Ardhuin*, 2001]. Under lower forcing conditions, relic ripples remain, but their effect on the waves is much weaker.

[30] **Acknowledgments.** This research is supported by the Coastal Dynamics Program of the Office of Naval Research and National Oceanographic Partnership Program (NOPP). We are grateful to the North Carolina Geological Survey for use of their side-scan sonar tow-fish. R. Dentzman (Aquamap) operated the equipment and supervised the surveys; his surveying and diving experience off the U.S. east coast was very valuable to our interpretation of the side-scan sonograms. We thank W. O'Reilly (SIO) and P. Jessen (NPS) for collecting and analyzing the directional wave buoy data. The National Data Buoy Center (NDBC, www.ndbc.noaa.gov) and the U.S. Army Corps Field Research Facility (FRF, www.frf.usace.army.mil) kindly provided the wave data from buoy 44014 and the 8 m depth array, respectively. The patience and dedication of the crew of R/V *Cape Hatteras* was greatly appreciated. Sediment samples were analyzed by Meg Dolan (FRF), Anne McElroy (NCSU), and Eric Patague (NPS). We thank T. Stanton and E. Thornton (NPS), J. McNinch (FRF), P. Traykovski (WHOI), and anonymous reviewers for insightful comments and discussions.

References

Andersen, K. H., The dynamics of ripples beneath surface waves and topics in shell models of turbulence, Ph.D. thesis, Univ. of Copenhagen, Copenhagen, 1999. (Available at http://mail.isva.dtu.dk/ken/Thesis.html.).

Andersen, K. H., and J. Fredsøe, How to calculate the geometry of vortex ripples, in *Coastal Sediments '99*, edited by N. C. Kraus and W. G. McDougal, pp. 78–93, Am. Soc. Civ. Eng., Reston. Va., 1999.

Ardhuin, F., Swell across the continental shelf, Ph.D. thesis, Naval Postgrad. Sch., Monterey, Calif., 2001. (Available at http://www.oc.nps.navy.mil/~ardhuin/index.html.).

Ardhuin, F., and T. H. C. Herbers, Bragg scattering of random surface gravity waves by irregular sea bed topography, *J. Fluid Mech.*, *451*, 1–33, 2001.

Ardhuin, F., T. H. C. Herbers, and W. C. O'Reilly, A hybrid Eulerian-Lagrangian model for spectral wave evolution with application to bottom friction on the continental shelf, *J. Phys. Oceanogr.*, *31*, 1498–1516, 2001.

Ayrton, H., The origin and growth of the ripple mark, *Proc. R. Soc. London, Ser. A*, *84*, 285 –310, 1910.

Bagnold, R. A., Motion of waves in shallow water, interaction between waves and sand bottoms, *Proc. R. Soc. London, Ser. A*, *187*, 1–15, 1946.

Blondeaux, P., Sand ripples under sea waves, 1, Ripple formation, *J. Fluid Mech.*, *218*, 1–17, 1990.

Darwin, G. H., On the formation of the ripple-mark in sand, *Proc. R. Soc. London, Ser. A*, *36*, 18–43, 1883.

Dingler, J. R., Wave-formed ripples in nearshore sands, Ph.D. thesis, Univ. of Calif., San Diego, Calif., 1974.

Faraci, C., and E. Foti, Evolution of small scale regular patterns generated by waves propagating over a sandy bottom, *Phys. Fluids*, *13*(6), 1624–1634, 2001.

Field, M. E., E. P. Meisburger, E. A. Stanley, and S. J. Williams, Upper quarternary peat deposit on the Atlantic inner shelf of the United States, *Geol. Soc. Am. Bull.*, *90*, 618–628, 1979.

Forel, F.-A., Rides formées à la surface du sable deposé au fond de l'eau, *Arch. Sci. Phys. Nat.*, *9*, 256, 1883.

Forel, F.-A., *Le Léman*, vol. II, 256 pp., Slatkine Reprints, Geneva, 1998.

Gallagher, E. L., S. Elgar, and E. B. Thornton, Megaripple migration in a natural surf zone, *Nature*, *394*(6689), 165–168, 1998.

Grant, W. D., and O. S. Madsen, Combined wave and current interaction with a rough bottom, *J. Geophys. Res.*, *84*, 1797–1808, 1979.

Grant, W. D., and O. S. Madsen, Movable bed roughness in unsteady oscillatory flow, *J. Geophys. Res.*, *87*, 469–481, 1982.

Green, M. O., Side-scan sonar mosaic of a sand ridge field: Southern mid-Atlantic bight, *Geo Mar. Lett.*, *6*, 35–40, 1986.

Hasselmann, K., et al., Measurements of wind-wave growth and swell decay during the Joint North Sea Wave Project, *Dtsch. Hydrogr. Z.*, *8*(12), 1–95, 1973.

Herbers, T. H. C., E. J. Hendrickson, and W. C. O'Reilly, Propagation of swell across a wide continental shelf, *J. Geophys. Res.*, *105*, 19,729–19,737, 2000.

Hunt, A. R., On the formation of the ripplemark, *Proc. R. Soc. London*, *34*, 1–18, 1882.

Lentz, S., R. T. Guza, S. Elgar, F. Feddersen, and T. H. C. Herbers, Momentum balances on the North Carolina inner shelf, *J. Geophys. Res.*, *104*, 18,205–18,226, 1999.

Lentz, S., M. Carr, and T. H. C. Herbers, Barotropic tides on the North Carolina shelf, *J. Phys. Oceanogr.*, *31*, 1843–1859, 2001.

Li, M. Z., and C. L. Amos, Sheet flow and large wave ripples under combined waves and currents: field observations, model predictions and effect on boundary layer dynamics, *Cont. Shelf Res.*, *19*, 637–663, 1999.

Madsen, O. S., and W. D. Grant, Quantitative description of sediment motion by waves, paper presented at the 15th International Conference on Coastal Engineering, Am Soc. Civ. Eng., Honolulu, Hawaii, 1976.

Madsen, O. S., P. P. Mathisen, and M. M. Rosengaus, Movable bed friction factors for spectral waves, paper presented at the 22nd International Conference on Coastal Engineering, Am Soc. Civ. Eng., Delft, Netherlands, 1990.

Madsen, O. S., L. D. Wright, J. D. Boon, and T. A. Chisholm, Wind stress, bed roughness and sediment suspension on the inner shelf during an extreme storm event, *Cont. Shelf Res.*, *13*, 1303–1324, 1993.

Milliman, J. D., O. H. Pilkey, and D. A. Ross, Sediments of the continental margin off the eastern United States, *Geol. Soc. Am. Bull.*, *83*, 1315–1333, 1972.

Mogridge, G. R., M. H. Davies, and D. H. Willis, Geometry prediction for wave-generated bedforms, *Coastal Eng.*, *22*(C11), 255–286, 1994.

Nielsen, P., Some basic concepts of wave sediment transport, *Tech. Rep. 20*, Inst. Strømningsmekanik Vandresurser, Danish Tech. Univ., Copenhagen, 1979.

Nielsen, P., Dynamics and geometry of wave-generated ripples, *J. Geophys. Res.*, *86*, 6467–6472, 1981.

Scott, J. T., and G. T. Csanady, Nearshore currents off Long Island, *J. Geophys. Res.*, *81*, 5401–5409, 1979.

Sherer, M. A., F. Melo, and M. Marder, Sand ripples in an oscillating annular sand-water cell, *Phys. Fluids*, *11*(1), 58–67, 1999.

Shields, A., Anwendung der ähnlichkeits-Mechanik und der Turbulenzforschung auf die Geschiebebewegung, *Preuss. Versuch. Wasserbau Schiffbau*, *26*, 524–526, 1936.

Soulsby, R. L., and R. J. S. W. Whitehouse, Threshold of sediment motion in coastal environments, paper presented at the Pacific Coasts and Ports Conference 1997, Univ. of Cantebury, Christchurch, New Zealand, 1997.

Southard, J. B., J. M. Lambie, D. C. Federick, H. T. Pile, and C. R. Wiedman, Experiments on bed configurations in fine sands under bidirectional purely oscillatory flow, and the origin of hummocky cross-stratification, *J. Sediment. Petrol.*, *60*, 1–17, 1990.

Swift, D. J. P., and P. Sears, Estuarine and littoral depositional patterns in the surficial sand sheet central and southern Atlantic shelf of North America, *Mém. Inst. Géol. Bassin Aquitaine*, *7*, 171–189, 1974.

Swift, D. J. P., J. W. Kofoed, F. P. Saulsbury, and P. Sears, Holocene evolution of the shelf surface, central and southern Atlantic shelf of North America, in *Shelf Sediment Transport: Process and Pattern*, chap. 23, pp. 499–574, John Wiley, New York, 1972.

Tolman, H. L., Wind waves and moveable-bed bottom friction, *J. Phys. Oceanogr.*, *24*, 994–1009, 1994.

Traykovski, P., A. E. Hay, J. D. Irish, and J. F. Lynch, Geometry, migration, and evolution of wave orbital ripples at LEO-15, *J. Geophys. Res.*, *104*, 1505–1524, 1999.

Vincent, C. E., and P. D. Osborne, Bedform dimensions and migration rates under shoaling and breaking waves, *Cont. Shelf Res.*, *13*, 1267–1280, 1993.

Vittori, G., and P. Blondeaux, Sand ripples under sea waves, 2, Finite-amplitude development, *J. Fluid Mech.*, *218*, 19–39, 1990.

Wallbridge, S., G. Voulgaris, B. N. Tomlison, and M. B. Collins, Initial motion and pivoting characteristics of sand particles in uniform and heterogeneous beds: Experiment and modelling, *Sedimentology*, *46*, 17–32, 1999.

Werner, B. T., and G. Kocurek, Bed-form dynamics: Does the tail wag the dog?, *Geology*, *25*(9), 771–774, 1997.

Wiberg, P. L., and C. K. Harris, Ripple geometry in wave-dominated environments, *J. Geophys. Res.*, *99*, 775–789, 1994.

Willis, D. H., M. H. Davies, and G. R. Mogridge, Laboratory observations of bedforms under directional irregular waves, *Rev. Can. Génie Civ.*, *20*, 550–563, 1993.

Wright, L. D., Micromorphodynamics of the inner continental shelf: A Middle Atlantic bight study, *J. Coastal Res.*, *15*, 93–130, 1993.

Wright, L. D., *Morphodynamics of inner continental shelves*, 241 pp., CRC Press, Boca Raton, Fla., 1995.

Young, I. R., and R. M. Gorman, Measurements of the evolution of ocean wave spectra due to bottom friction, *J. Geophys. Res.*, *100*, 10,987–11,004, 1995.

Zhukovets, A. M., The influence of bottom roughness on wave motion in a shallow body of water, *Izv. Akad. Nauk. SSR*, *10*, 1561–1570, 1963.

F. Ardhuin, Centre Militaire d'Océanographie, Service Hydrographique et Océanographique de la Marine, F-29609 Brest, France. (ardhuin@shom.fr)

T. G. Drake, Department of Marine, Earth and Atmospheric Sciences, North Carolina State University, Raleigh, NC 27695-8208, USA. (drake@ncsu.edu)

T. H. C. Herbers, Department of Oceanography, Naval Postgraduate School, Monterey, CA 93943-5122, USA. (herbers@oc.nps.navy.mil)